Human influence on the increasing drought risk over Southeast Asian monsoon region

Lixia Zhang[1], Ziming Chen[2], and Tianjun Zhou[3]

[1]LASG, Institute of Atmospheric Physics Chinese Academy of Sciences
[2]LASG, Institute of Atmospheric Physics, Chinese Academy of Sciences
[3]IAP

November 22, 2022

Abstract

Southeast Asian monsoon region is regularly stricken by drought, but less attention is paid due to its slow-onset and less visual impact. This study investigated the observed drought changes over Southeast Asian monsoon region and impacts of anthropogenic forcing using the Coupled Model Intercomparison Project phase 6 (CMIP6) models. We revealed an increasing drought risk for 1951-2018 due to more frequent and wide-spread droughts. The influence of anthropogenic forcing is successfully detected, which has increased the likelihood of the extreme droughts in historical simulation by reducing precipitation and enhancing evapotranspiration. The time of emergence of anthropogenic forcing in extreme drought occurrence and affected area occurs around the 1960s. The future projected severe and extreme drought risks are still beyond natural only forced changes under all scenarios. Our findings demonstrate a robust impact of anthropogenic forcing on drought risk over Southeast Asia, and highlight the importance of future pathway choice.

Table S1 CMIP6 models and the years of their piControl simulation used in this study

Model	**Institute/Country**	**Lat x Lon**	**piControl**	**Reference**
BCC-CSM2-MR	BCC-CMA/China	160 x 320	600	Wu et al. (2019)
CNRM-CM6-1	CNRM-CERFACS/France	128 x 256	500	Voldoire et al. (2019).
CNRM-ESM2-1	CNRM-CERFACS/France	128 x 256	500	Séférian et al. (2019)
CanESM5	CCCMA/Canada	64 x 128	1000	Swart et al. (2019)
EC-Earth3	EC-Earth-Consortium/Europe	256 x 512	501	Haarsma et al. (2020)
FGOALS-g3	LASG-IAP/China	90x180	700	Li et al. (2020)
GFDL-ESM4	NOAA-GFDL/USA	180 x 360	500	Dunne et al. (2020)
INM-CM4-8	INM/Russia	120X180	531	Volodin, et al. (2018)
IPSL-CM6A-LR	IPSL/France	143 x 144	1200	Boucher et al. (2019)
MIROC6	MIROC/Japan	128 x 256	800	Tatebe et al. (2019)
MPI-ESM1-2-HR	MPI-M/Germany	192 x 384	500	Müller et al. (2018)
MPI-ESM1-2-LR	MPI-M/Germany	96 x 192	1000	Mauritsen et al. (2019)
MRI-ESM2-0	MRI/Japan	96 x 192	701	Yakimoto et al. (2019)
UKESM1-0-LL	MOHC/UK	144 x 192	1100	Sellar et al. (2019)

Table S2 Number of realizations for the historical and future projection

Model	Historical	SSP1-2.6	SSP2-4.5	SSP3-7.0	SSP5-8.5
BCC-CSM2-MR	3	1	1	1	1
CNRM-CM6-1	10	6	6	6	6
CNRM-ESM2-1	5	5	5	5	5
CanESM5	25	14	10	10	10
EC-Earth3	1	1	1	1	1
FGOALS-g3	1	1	1	1	1
GFDL-ESM4	1	1	1	1	1
INM-CM4-8	1	1	1	1	1
IPSL-CM6A-LR	9	5	5	5	5
MIROC6	10	10	3	3	10
MPI-ESM1-2-HR	1	1	1	1	1
MPI-ESM1-2-LR	1	1	1	1	1
MRI-ESM2-0	1	1	1	1	1
UKESM1-0-LL	1	1	1	1	1

Table S3 TOE (unit: year) of precipitation (P), evapotranspiration (ET) and P minus ET (PmE) area-averaged over the Southeast Asian monsoon region firstly occurs in Hist (first row). The numbers for SSP1-2.6, SSP2-4.5, SSP3.0 and SSP5-8.5 are the years when the external forced changes fall in the range of internal variability in the future projection. The ranges in the parenthesis denote the ±1 standard deviation. "—" means the external forced changes never return to natural variability in the future.

Scenarios	P	ET	PmE
Hist	1980 (1973~1987)	1999(1968-2030)	1981 (1973~1989)
SSP1-2.6	2030 (2025~2035)	—	2049 (2041~2057)
SSP2-4.5	2037 (2031~2043)	—	—
SSP3-7.0	2059 (2054~2064)	—	—
SSP5-8.5	2039 (2032~2046)	—	2078 (2061~2095)

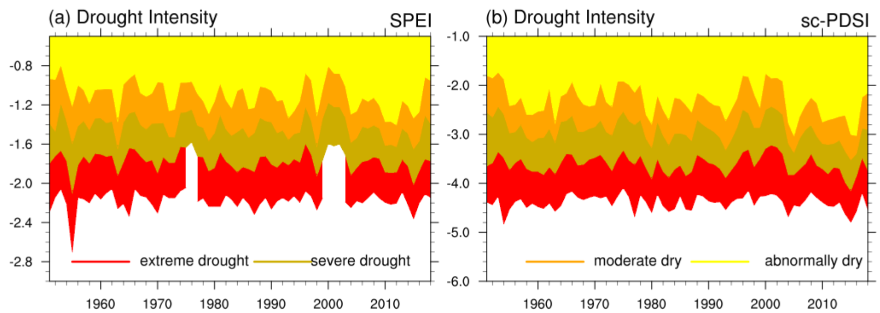

Fig.S1 The temporal changes of drought intensity for different drought categories averaged over Southeast Asian land monsoon region (10-30°N, 90-120°E) based on (a) SPEI, and (b) sc-PDSI. The yellow, orange, brown and red lines represent abnormally dry (SPEI[?]-0.5, sc-PDSI[?]-1.0), moderate drought (SPEI[?]-1.0, sc-PDSI[?]-2.0), severe drought (SPEI[?]-1.5, sc-PDSI[?]-3.0), and extreme drought (SPEI[?]-2.0, sc-PDSI[?]-4.0), respectively.

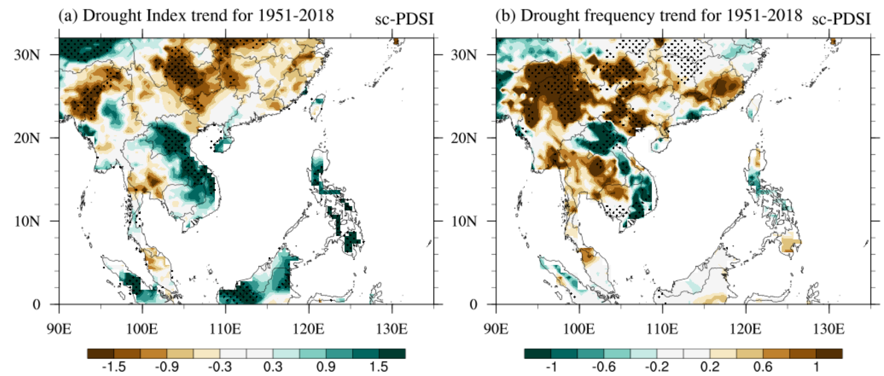
(a) Drought Index trend for 1951-2018
sc-PDSI
30N
20N
10N
0
90E
100E
110E
120E
130E
-1.5
-0.9
-0.3
0.3
0.9
1.5
(b) Drought frequency trend for 1951-2018
sc-PDSI
-1
-0.6
-0.2
0.2
0.6
1

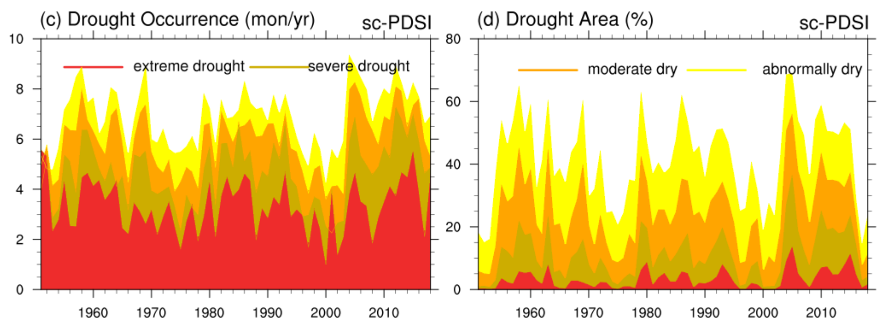

Fig.S2 Same as Fig.1, but for the results based on sc-PDSI.

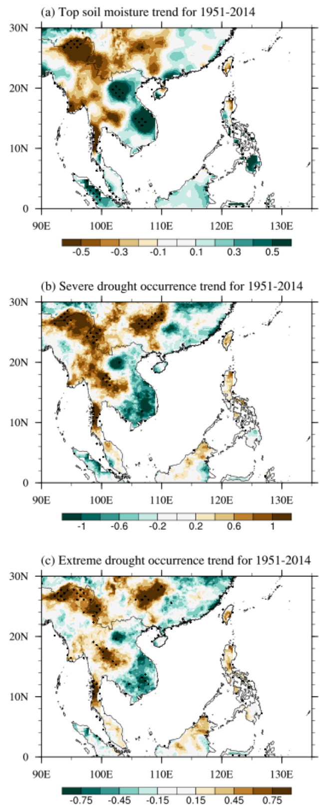

Fig. S3 The linear trend of (a) surface soil moisture (0-10cm soil moisture content, unit: kg $m^{-2}68yr^{-1}$), (b) severe drought occurrence (unit: mon $68yr^{-1}$), (c) extreme drought occurrence (unit: mon $68yr^{-1}$) for 1951-2014 derived from GLDAS dataset. To minimize the geophysical discrepancy of soil moisture, we standardized the surface soil moisture anomalies and then use the standardized results to characterize drought. A severe and extreme drought event is a month with the surface soil moisture less than -1.5 and -2.0 standard deviation, respectively. This approach adopted here is similar to Sohrabi et al. (2015), but only employs surface soil moisture.

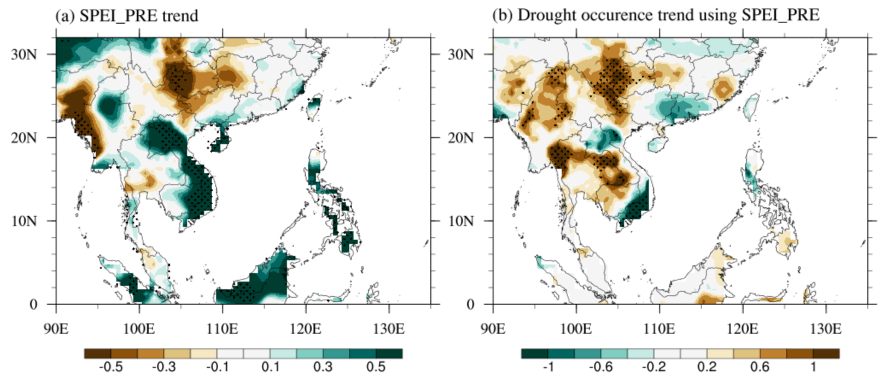

(a) SPEI_PRE trend
30N
20N
10N
0
90E
100E
110E
120E
130E
-0.5
-0.3
-0.1
0.1
0.3
0.5
(b) Drought occurence trend using SPEI_PRE
30N
20N
10N
0
90E
100E
110E
120E
130E
-1
-0.6
-0.2
0.2
0.6
1

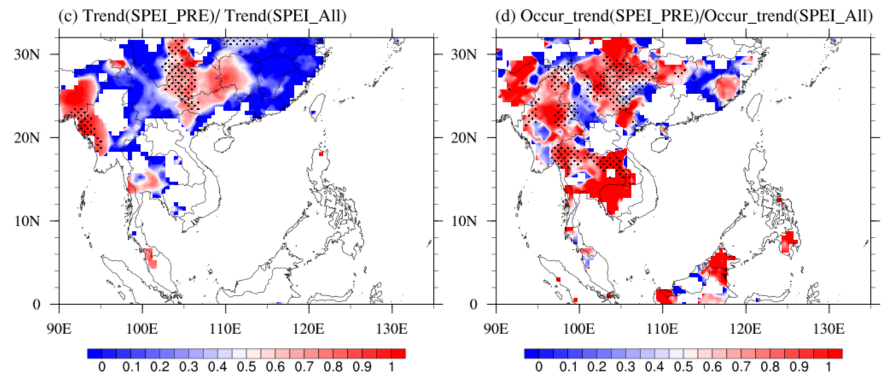

Fig.A4 (a)-(b), same as Fig.1a-b, bur for the results derived from SPEI_PRE. (c) The ratio of the linear trend of SPEI_PRE to that of SPEI_All. (d) the ratio of the linear trend of extreme drought occurrence derived from SPEI_PRE to that derived from SPEI_All. The original SPEI with both changes in precipitation and ET is referred as SPEI_All. SPEI_PRE is similar to SPEI_All, but calculated from the detrended ET for 1901-2018 and the original precipitation (Cook et al. 2014). When the ratio in (c)-(d) is higher than 0.5, it indicates the contribution of precipitation changes is higher than that of ET.

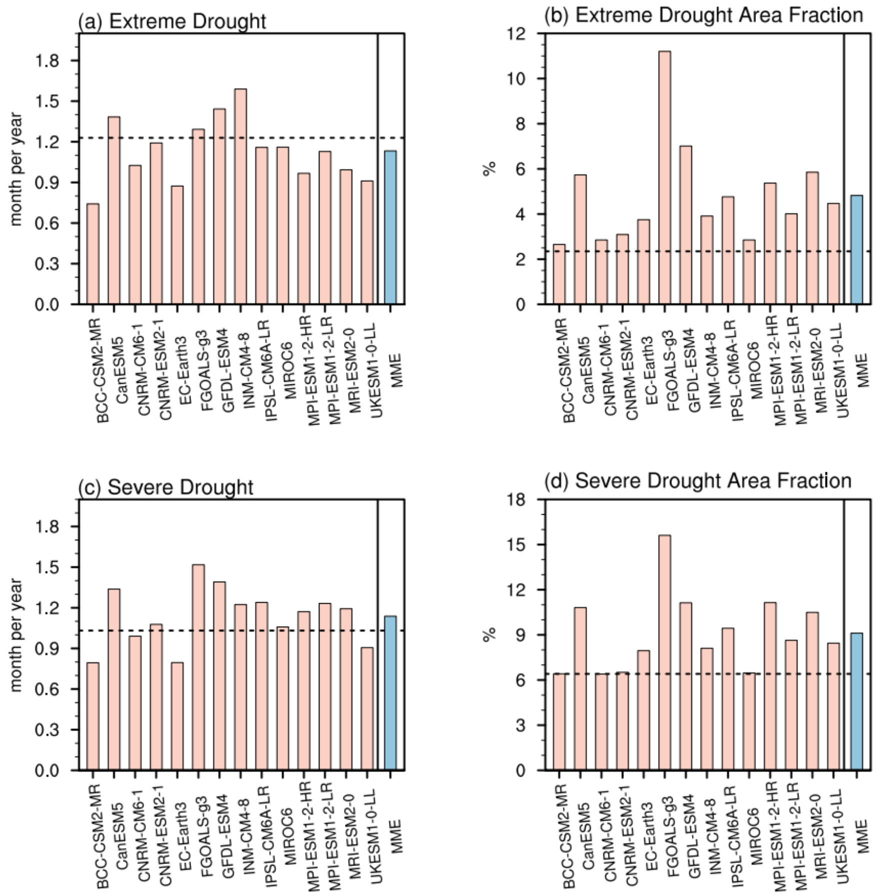

Fig. S5 The standard deviation of (a) extreme drought occurrence (unit: mon per year) and (b) area fraction (unit: %) from 1950 to 2014 from the observation (dash lines) and the historical run of the 14 CMIP6 models (bar) for 1951-2014. The blue bars denote the multi-model ensemble mean (MME). The 20-yr running mean has been carried out before calculating the standard deviation. (c) and (d) are same as (a) and (b) but for the severe drought.

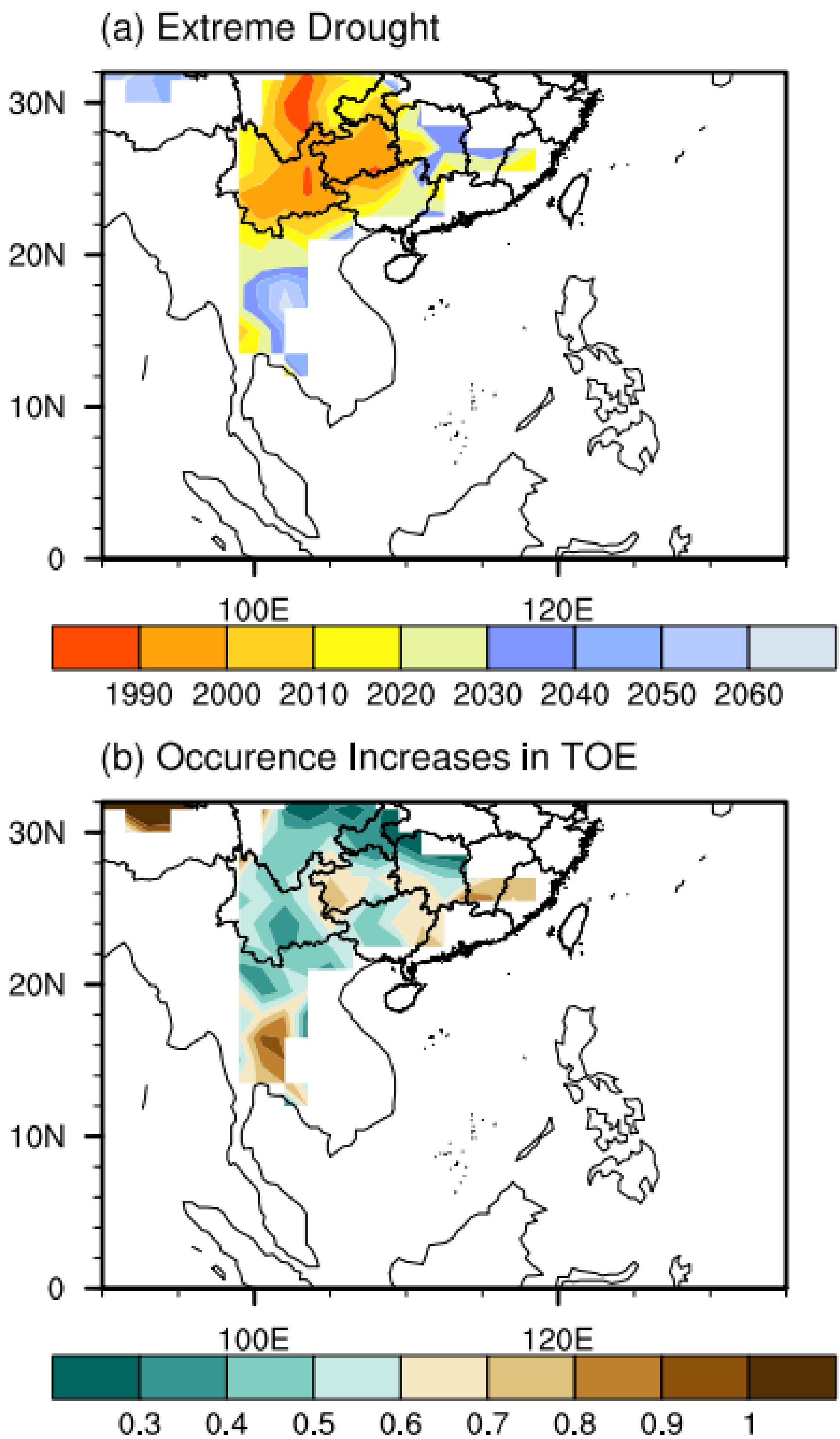

Fig. S6 (a) The spatial distribution of TOE for extreme drought occurrence firstly appeared in Hist and (b) the anomalies of extreme drought frequency (unit: mon year^{-1}) averaged over the 20-yr around TOE relative to piControl. The white areas denote that the TOE does not exist.

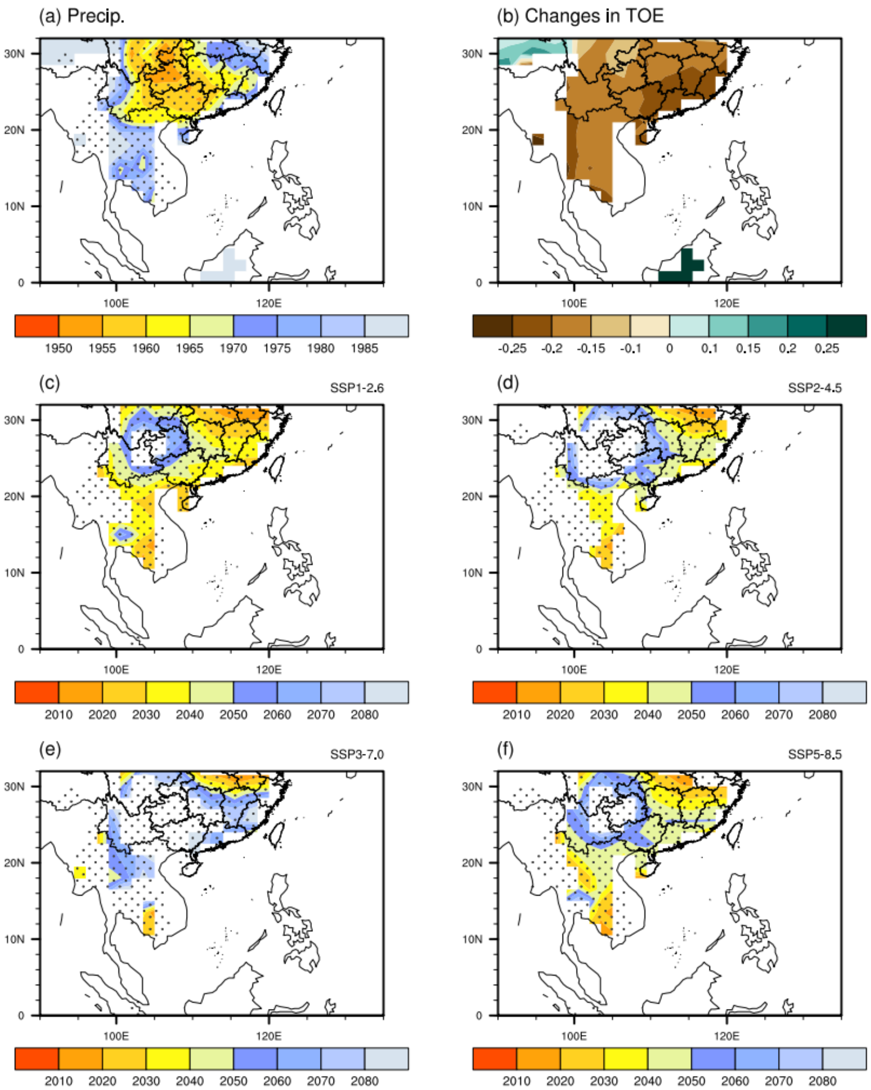

Fig.S7 (a)-(b) are the same as Fig.S6, but for precipitation. (c)-(f) are the years when changes in precipitation return to the ranges of internal variability. The stippling denotes that precipitation decreases exceed the range of internal variability in the TOE.

Reference:

Boucher, O., Servonnat, J., Albright, A. L., Aumont, O., Balkanski, Y., Bastrikov, V., et al. (2020). Presentation and evaluation of the IPSL-CM6A-LR climate model. Journal of Advances in Modeling Earth Systems, 12, e2019MS002010.*https://doi.org/10.1029/2019MS002010*

Dunne, J. P., Horowitz, L. W., Adcroft, A. J., Ginoux, P., Held, I. M., John, J. G., & Zhao, M. (2020). The GFDL Earth System Model version 4.1 (GFDL-ESM4.1): Overall coupled model description and simulation characteristics. Journal of Advances in Modeling Earth Systems, 12, e2019MS002015.*https://doi.org/10.1029/2019MS002015*

Haarsma, R., Acosta, M., Bakhshi, R., Bretonnière, P.-A., Caron, L.-P., Castrillo, M., Corti, S., Davini, P., Exarchou, E., Fabiano, F., Fladrich, U., Fuentes Franco, R., García-Serrano, J., von Hardenberg, J., Koenigk, T., Levine, X., Meccia, V. L., van Noije, T., van den Oord, G., Palmeiro, F. M., Rodrigo, M., Ruprich-Robert, Y., Le Sager, P., Tourigny, E., Wang, S., van Weele, M., and Wyser, K. (2020): HighResMIP versions of EC-Earth: EC-Earth3P and EC-Earth3P-HR – description, model computational performance and basic validation, Geosci. Model Dev., 13, 3507–3527, https://doi.org/10.5194/gmd-13-3507-2020

Li, L. J., Yu, Y. Q., Tang, Y. L., Lin, P., Xie, J., Song, M., et al. (2020). The flexible global ocean–atmosphere–land system model grid-point version 3 (FGOALS-g3): Description and evaluation. Journal of Advances in Modeling Earth Systems, 12(9).*https://doi.org/10.1029/2019MS002012*

Mauritsen T, Bader J, Becker T, Behrens J, Bittner M, Brokopf R, Brovkin V, Claussen M, Crueger T, Esch M, Fast I, Fiedler S, Flaschner D, Gayler V, Giorgetta M, Goll DS, Haak H, Hagemann S, Hedemann C, Roeckner E (2019) Developments in the MPI-M earth system model version 1.2 (MPI-ESM1.2) and its response to increasing CO2. J Adv Model Earth Syst. https://doi.org/10.1029/2018MS001400

Muller, W. A., Jungclaus, J. H., Mauritsen, T., Baehr, J., Bittner, M., Budich, R., & Marotzke, J. (2018). A higher-resolution version of the Max Planck Institute Earth System Model (MPI-ESM1.2-HR). Journal of Advances in Modeling Earth Systems, 10(7), 1383– 1413. https://doi.org/10.1029/2017MS001217

Seferian, R., Nabat, P., Michou, M., Saint-Martin, D., Voldoire, A., Colin, J., Decharme, B., Delire, C., Berthet, S., Chevallier, M., Senesi, S., Franchisteguy, L., Vial, J., Mallet, M., Joetzjer, E., Geoffroy, O., Gueremy, J., Moine, M., Msadek, R., Ribes, A., Rocher, M., Roehrig, R., Salas-y-Melia, D., Sanchez, E., Terray, L., Valcke, S., Waldman, R., Aumont, O., Bopp, L., Deshayes, J., Ethe, C., and Madec, G.(2019): Evaluation of CNRM Earth System Model, CNRM-ESM2-1: Role of Earth System Processes in Present-Day and Future Climate, J. Adv. Model. Earth Syst., 11, 4182–4227, https://doi.org/10.1029/2019MS001791.

Sellar, A. A., Jones, C. G., Mulcahy, J., Tang, Y., Yool, A., Wiltshire, A., O'Connor, F. M., Stringer, M., Hill, R., Palmieri, J., Woodward, S., Mora, L., Kuhlbrodt, T., Rumbold, S., Kelley, D. I., Ellis, R., Johnson, C. E., Walton, J., Abraham, N. L., Andrews, M. B., Andrews, T., Archibald, A. T., Berthou, S., Burke, E., Blockley, E., Carslaw, K., Dalvi, M., Edwards, J., Folberth, G. A., Gedney, N., Griffiths, P. T., Harper, A. B., Hendry, M. A., Hewitt, A. J., Johnson, B., Jones, A., Jones, C. D., Keeble, J., Liddicoat, S., Morgenstern, O., Parker, R. J., Predoi, V., Robertson, E., Siahaan, A., Smith, R. S., Swaminathan, R., Woodhouse, M. T., Zeng, G., and Zerroukat, M. (2019): UKESM1: Description and evaluation of the UK Earth System Model, J. Adv. Model. Earth Syst., 11, 4513–4558, https://doi.org/10.1029/2019ms001739.

Sohrabi M.M., Ryu J.H., Asece M., Abatzoglou J., J. Trach (2015): Development of Soil Moisture Drought Index to Characterize Droughts. J. Hydrol. Eng. 20 (11): 04015025. DOI: 10.1061/(ASCE)HE.1943-5584.0001213.

Swart, N. C., Cole, J. N. S., Kharin, V. V., Lazare, M., Scinocca, J. F., Gillett, N. P., Anstey, J., Arora, V., Christian, J. R., Hanna, S., Jiao, Y., Lee, W. G., Majaess, F., Saenko, O. A., Seiler, C., Seinen, C., Shao, A., Sigmond, M., Solheim, L., von Salzen, K., Yang, D., and Winter, B.(2019): The Canadian Earth System Model version 5 (CanESM5.0.3), Geosci. Model Dev., 12, 4823–4873, https://doi.org/10.5194/gmd-12-4823-2019.

Tatebe, H., Ogura, T., Nitta, T., Komuro, Y., Ogochi, K., Takemura, T., Sudo, K., Sekiguchi, M., Abe, M., Saito, F., Chikira, M., Watanabe, S., Mori, M., Hirota, N., Kawatani, Y., Mochizuki, T., Yoshimura, K., Takata, K., O'ishi, R., Yamazaki, D., Suzuki, T., Kurogi, M., Kataoka, T., Watanabe, M., and Kimoto, M.(2019): Description and basic evaluation of simulated mean state, internal variability, and climate sensitivity in MIROC6, Geosci. Model Dev., 12, 2727–2765, https://doi.org/10.5194/gmd-12-2727-2019.

Voldoire, A., SaintMartin, D., Senesi, S. D. B., Alias, A., & Chevallier, e. a., M. (2019). Evaluation of CMIP6 DECK experiments with CNRMCM61. Journal of Advances in Modeling Earth Systems, 11, 2177–2213.*https://doi.org/10.1029/2019MS001683*

Volodin Evgenii M., Evgeny V. Mortikov , Sergey V. Kostrykin , Vener Ya. Galin, Vasily N. Lykossov , Andrey S. Gritsun , Nikolay A. Diansky , Anatoly V. Gusev , Nikolay G. Iakovlev , Anna A. Shestakova and

Svetlana V. Emelina (2018). Simulation of the modern climate using the INM-CM48 climate model. Russ. J. Numer. Anal. Math. Modelling 2018; 33(6):367–374. Doi: 10.1515/rnam-2018-0032

Wu, T., Lu, Y., Fang, Y., Xin, X., Li, L., Li, W., Jie, W., Zhang, J., Liu, Y., Zhang, L., Zhang, F., Zhang, Y., Wu, F., Li, J., Chu, M., Wang, Z., Shi, X., Liu, X., Wei, M., Huang, A., Zhang, Y., and Liu, X.(2019): The Beijing Climate Center Climate System Model (BCC-CSM): the main progress from CMIP5 to CMIP6. Geosci. Model Dev., 12, 1573–1600, https://doi.org/10.5194/gmd-12-1573-2019.

Yukimoto, S., H. Kawai, T. Koshiro, N. Oshima, K. Yoshida, S. Urakawa, H. Tsujino, M. Deushi, T. Tanaka, M. Hosaka, S. Yabu, H. Yoshimura, E. Shindo, R. Mizuta, A. Obata, Y. Adachi, and M. Ishii (2019): The Meteorological Research Institute Earth System Model version 2.0, MRI-ESM2.0: Description and basic evaluation of the physical component. J. Meteor. Soc. Japan, 97, 931–965, doi:10.2151/jmsj.2019-051.

Human influence on the increasing drought risk over Southeast Asian monsoon region

Lixia Zhang[1, 2], Ziming Chen[1,3] and Tianjun Zhou[1, 3]

1 LASG, Institute of Atmospheric Physics, Chinese Academy of Sciences, Beijing, China

2 Collaborative Innovation Center on Forecast and Evaluation of Meteorological Disasters, Nanjing University of Information Science & Technology, Nanjing, 210044, China

3 University of Chinese Academy of Sciences, Beijing 100049, China

Submitted to GRL

Revised on 8th April, 2021

Corresponding author: Lixia Zhang (lixiazhang@mail.iap.ac.cn)

Key points:

- Drought occurrence and affected area over Southeast Asian monsoon region has been increasing since 1951 in the observation.
- The human influence on the historical changes of drought risk over Southeast Asian monsoon region is detectable.
- The time of emergence of anthropogenic forcing in extreme drought occurrence and affected area occurs in the 20^{th} century.

Abstract: Southeast Asian monsoon region is regularly stricken by drought, but less attention is paid due to its slow-onset and less visual impact. This study investigated the observed drought changes over Southeast Asian monsoon region and impacts of anthropogenic forcing using the Coupled Model Intercomparison Project phase 6 (CMIP6) models. We revealed an increasing drought risk for 1951-2018 due to more frequent and wide-spread droughts. The influence of anthropogenic forcing is successfully detected, which has increased the likelihood of the extreme droughts in historical simulation by reducing precipitation and enhancing evapotranspiration. The time of emergence of anthropogenic forcing in extreme drought occurrence and affected area occurs around the 1960s. The future projected severe and extreme drought risks are still beyond natural only forced changes under all scenarios. Our findings demonstrate a robust impact of anthropogenic forcing on drought risk over Southeast Asia, and highlight the importance of future pathway choice.

Key Words: Drought risk, Southeast Asia monsoon, CMIP6, Time of Emergence

Plain Language Summary:

As a humid region, drought in Southeast Asian monsoon region is often underestimated due to its slow rate of onset and less visual impact. Here we revealed a significant increasing trend of drought occurrence and affected area over Southeast Asian monsoon region since the 1950s. The impact of human influence is successfully detected using the Coupled Model Intercomparison Project phase 6 (CMIP6) models. Anthropogenic forcing has increased the likelihood of the extreme droughts for 1951-2014 by suppressing water supply and enhancing evaporation demand. The time of emergence of anthropogenic forcing in extreme drought frequency and affected area firstly appeared around the 1960s. Even though drought risk will start to decrease since the 2030s in the future under the lowest emission scenario of CMIP6, the projected drought risks are still beyond natural only forced changes.

1. Introduction

Southeast Asian monsoon region falls in the warm and humid tropics modulated by Asian monsoon. It is home to nearly 15% of the world's tropical forests and 8.5% population in 3% earth's total land area, and also one of the biodiversity hotspots in the world (Stibig et al., 2014; Sodhi et al., 2010). With the unprecedented urbanization and population growing rate, water scarcity issues have already posed a serious challenge for sustainable development in Southeast Asian monsoon region (Kumar et al., 2015). As a humid region, drought in this region is often underestimated due to its slow rate of onset and less visual impact. However, drought can have devastating cumulative impacts, especially on the countries which are poor and less developed but heavily depend on agriculture (Polpanich, 2010). Thus, understanding the drought changes and the behind mechanism are of great importance.

This study focuses on the Southeast Asian monsoon region, including the mainland Southeast Asian countries and South China (10~30°N, 90~120°E) (Fig.1a-b), because this region has the longest wet season and the strongest interannual variability in the monsoon length in the Asian monsoon region (Misra and DiNapoli 2013). Decreasing trends in annual precipitation from the 1950s to 2000s were observed in Myanmar, Thailand and northern Vietnam (Endo et al., 2009), and the number of rainy days was significantly decreased over Southeast Asia from 1961 to 1998 (Manton et al., 2001). Drought has affected over 66 million people in Southeast Asian countries for the past 30 decades (ASEAN, 2019). The 2020 drought started from 2019 has caused water levels in Southeast Asia's Mekong River to drop to its lowest in more than 100 years (https://www.nationalgeographic.com/environment/2019/07/mekong-river-lowest-levels-100-years-food-shortages/), affecting 13 provinces in the Mekong Delta region (https://reliefweb.int/report/viet-nam/viet-nam-drought-and-saltwater-intrusion-office-resident-coordinator-flash-update-1). The 2020 drought also spread to Southwest China, the upstream of Mekong River, and over one million people were lack of accessing drinking water (https://news.cgtn.com/news/2020-04-05/Drought-affects-over-one-million-people-in-SW-China-province-PrpBkhlJok/index.html). South China, adjacent to the Southeast Asian countries, has been frequently stricken by droughts in recent decades (Xin et al., 2008; Zhang et al., 2013; Chen and Sun, 2015; Zhang et al., 2020). The two adjacent regions share the same climate and are facing similar drought risk. Thus, we study the drought changes over the traditional Southeast Asian countries and South China together in this study.

Climate change could further aggravate drought by either enhancing evapotranspiration or suppressing precipitation (Dai, 2011; Trenberth et al., 2014), and Southeast Asian monsoon region is one of the hotspots with strong drying under global warming (Cook et al., 2020). The effect of black carbon aerosol radiative forcing can partly explain the observed drying trend of Southeast Asian spring precipitation (Lee and Kim, 2010). The optimal fingerprinting attribution shows a dominant role of anthropogenic aerosols forcing in the declining trend since the 1950s of northern hemispheric monsoon precipitation, including Southeast Asia (Polson et al., 2014). Compared with present-day, drought events are projected to increase in the future over mainland Southeast Asia based on the regional climate model (Amnuaylojaroen and Chanvichit, 2019) and CMIP5 multimodel simulations (Lu et al., 2019). As for the droughts associated with El Niño events, drought would cover more area over Southeast Asia in thenear future even with less severe El Niño events, and droughts associated with severe El Niño would be more extreme and more widely spread in the near and far future (Hariadi, 2017).

The Coupled Model Intercomparison Project phase 6 (CMIP6) with improved climate models and more modelling groups is expected to provide more reliable information on the regional climate response to anthropogenic forcing (Eyring et al., 2016; Ukkola et al., 2020). This study aims to answer the following questions by examining observation and CMIP6 multimodel output: 1) How does the observed drought over Southeast Asian monsoon region change since the 1950s? 2)Whether anthropogenic forcing plays any role in the drought changes? 3) How would drought change under different scenarios in the future?

2. Data and Method

2.1 Observation and CMIP6 model simulations

We use monthly observational precipitation and potential evapotranspiration dataset from the Climatic Research Unit of the University of East Anglia (CRU TS v.4.03) for 1951-2018 at a horizontal resolution of 0.5º (Harris et al., 2020). To verify the observed drought changes revealed by SPEI, the surface (0-10cm) soil moisture from Global Land Data Assimilation System Version 2 (GLDAS-2.0, Rodell et al. 2004; Beaudoing et al. 2019) for 1951-2014 is also used. We employ the pre-industrial control simulation (piControl), historical simulation (Hist) and four future scenarios projections from 14 coupled models underpin CMIP6 to explore the role of anthropogenic forcing and the scenario dependence of drought changes in future projection (Table S1-2). The four scenarios chosen in this study are the Shared Socioeconomic Pathways (SSP) 1-2.6, 2-4.5, 3-7.0 and 5-8.5 (O'Neill et al., 2016). The piControl is employed to estimate internal variability of the unforced drought. All model outputs are interpolated onto the same resolution of 1.5°×1.5° using the first-order conservative interpolation. We use Hargreaves equation to calculate reference evapotranspiration (ET) (Hargreaves, 1994), which has a good agreement with Penman-Monteith method (Droogers and Allen, 2002).

This study chooses the Standardized Precipitation-Evapotranspiration Index (SPEI, Vicente-Serrano et al., 2010a, b) to investigate the changes in drought intensity, occurrence or frequency defined as drought months per year and affected area fraction. To verify the observed drought changes revealed by SPEI, self-calibrating Palmer Drought Severity Index (sc-PDSI, Wells et al., 2004) is also employed. In observation, SPEI and sc-PDSI are both calculated based on the CRU TSv.4.03 precipitation and evapotranspiration dataset (Vicente-Serrano et al., 2010b; Schrier et al., 2013). As monthly sc-PDSI is not able to depict drought on time scales shorter than 12 months, we use SPEI at a 12-month time scale to estimate drought changes in the observation. In each model simulation, SPEI is calculated using a Log-Logistic distribution (Vicente-Serrano et al., 2010a), the parameters of which are derived by fitting it to the piControl simulations of that model.

2.2 Estimate of internal variability and Time of Emergence

Following Zhang and Delworth (2018), internal variability is estimated from multi-millennia preindustrial control simulations. For drought occurrence and affected area changes, we first calculate the drought occurrence at each grid and the drought affected area of the study area. The running-mean drought affected area and area-averaged drought frequency for a 20-yr period over the target region are then calculated. Internal variability is defined as the range between the maximum and minimum values across the entire piControl runs, respectively. The results are only caused by internal climate variability. For internal variability of the changes in precipitation, we first randomly select two non-overlapping 20-yr periods from the piControl simulation. Then, we calculate the difference between these two 20-yr periods. Next, we repeat these 14 times (to mimic the 14 models ensemble) to form the ensemble and compute ensemble average. Finally, we repeat the above process 5000 times to gain a probability density function (PDF) of internal variability.

The time of emergence (TOE) is defined as the time when external forcing signal, which is represented by multimodel ensemble mean (MME), exceeds internal variability firstly and lasts at least 2 decades (Zhang and Delworth 2018). To estimate the spread of TOE, we calculate the time when the MME exceeds ranges of internal variability of each model, and define this time as the TOE for each model. The spread of TOE is the range of ±1 standard deviation of TOE across the 14 models.

3. Results

3.1 Observed drought changes for 1951-2018

In observation, an overall drying trend over the Southeast Asian monsoon region is observed since the 1950s, with the strongest drying trend over Yunnan Province in China, northern Thailand and Myanmar (Fig.1a). SPEI has decreased by -0.75 at the maximum from 1951 to 2018. The occurrence of extreme drought, defined as month with SPEI≤-2.0 per year, has been significantly increasing over the regions with significant decreasing trend of SPEI (Fig.1b). It is centered over the Southwest China and Burma. In contrast, Viet Nam, along the east coast of Pacific Ocean, show significant wetting trends. Significant increasing trends in the drought occurrence and affected area are seen from the temporal changes averaged over Southeast Asia (Fig.1c-d). For the past 68 years, the severe and extreme drought occurrence (affected area) has increased by 0.8 and 0.2 month per year (7.1% and 3.1%), respectively, approximately 23% and 8% (85% and 142%) of climate mean. In contrast, the linear trend in drought intensity is insignificant (Fig.S1a). So, we will mainly focus on the changes in drought occurrence and affected area in the following sections.

The results based on sc-PDSI (Fig.S1b and Fig.S2) and surface soil moisture (Fig.S3) both confirm the increasing drought risk over Southeast Asian monsoon region. Following Cook et al. (2014), we recalculate SPEI by removing the linear trend of ET for 1901-2018 to estimate contribution of precipitation changes to the drought risk trend (Fig.S4). Over the centers with strongest decreasing trend of SPEI and increasing trend of drought occurrence, the contribution of precipitation changes is higher than 50%, reaching 0.9 at maximum, demonstrating the importance of precipitation changes. Given the high consistency between sc-PDSI and SPEI, we will use SPEI to investigate the impact of anthropogenic forcing in the following discussion.

3.2 Responses of droughts to historical anthropogenic forcing

By comparing PDF distributions of drought indices averaged over the study region in Hist and piControl, a detectable role of anthropogenic forcing can be seen from the leftward (rightward) shift in SPEI, precipitation and surface soil moisture (ET, drought occurrence and affected area) under anthropogenic forcing (Fig.2a-b). The likelihood of a 1-in-20-yr drought event defined by extreme drought occurrence and affected area in piControl is estimated to increase to 24% (6%~49% for 10th-90th confidence level) and 32% (25% to 45%) in Hist, respectively. It indicates anthropogenic forcing has increased the risk of such event by 5-time (3~25-time) and 6-time (4~9-time) estimated from risk ratio ($P_{Hist}/P_{piControl}$), respectively. Human influence can intensify the drought risk by increasing both standard deviation and climate mean of precipitation, ET and SPEI (horizontal lines Fig.2a-c). Specifically, standard deviation for SPEI, precipitation anomaly and ET anomaly in Hist increases to 0.44, 0.81 mm day^{-1}, and 0.15 mm day^{-1} from 0.40, 0.77 mm day^{-1}, and 0.13 mm day^{-1} in piControl.

3.3 ToE of anthropogenic forcing

To investigate when the human influence forced signal exceeds natural variability, we estimate the TOE of anthropogenic forcing here. Because estimation of TOE is sensitive to the simulated ranges of climate variability, we firstly evaluate the models' capability in simulating the variability of drought occurrence and affected area over Southeast Asian monsoon region. Most CMIP6 models and MME underestimate the variability of occurrence of extreme drought, but overestimate the extreme and severe drought affected area fraction (Fig.S5). To avoid the model biases, we scale the simulated variability of internal variability using the ratio between the standard deviation of observation and of Hist of each model for the period 1950-2018.

Consistent with the observation, a significant increasing trend for the drought occurrence and affected area fraction since the early 20th century is clearly simulated in Hist. The TOE of climate change induced extreme drought occurrence and affected area emerges around 1967 (1928~2006) and 1967 (1941~1993), close to that of severe drought events 1969 (1935~2003) and 1967 (1939~1995). We also investigate whether future changes in drought risk under different scenarios will return to natural only forced variability (colored lines in Fig.3). The extreme and severe drought occurrence and area fraction start to decrease around the 2030s under SSP1-2.6 and keep stable since the 2030s under SSP2-4.5, while continue to increase through the whole 21st century under SSP3-7.0 and SSP5-8.5. The anthropogenic forced higher drought risks are still beyond the ranges of natural variability of piControl under the four scenarios, although a decrease is shown in SSP1-2.6. The largest increase is seen from SSP3-7.0, which has the greatest anthropogenic aerosol loadings in the future (Wilcox et al. 2020). The drought will become more frequent and more widespread in the future compared with piControl under all scenarios, but a slight decrease relative to present day is projected under the lowest emission scenarios. The earliest TOE has appeared over the Southwest China before the 1990s, followed by the Mekong river basin countries

(Fig.S6a). For the drought occurrence changes averaged over the 20 years around TOE relative to piControl, extreme drought increases by 0.4 ~ 0.8month per year over the Southwest China and 0.4~1 month over Thailand (Fig.S6b).

We also present the changes of precipitation, ET and their difference (PmE) relative to piControl to see their impact on drought risk changes(Fig.4). In the 20^{th} century, the ensemble mean precipitation of the 14 CMIP6 models shows very similar evolution to those in drought, decreasing with time from the early 21^{st} century to present, reaching its minimum recently. The TOE of precipitation occurs around 1980 (1973~1987) (Fig.4a). Meanwhile, the anthropogenic activity forced ET increases with time and goes beyond natural variability around 1999 (1968~2030), with much weaker magnitude than precipitation (Fig.4b). The combination of decrease in water supply (precipitation) and increase in evaporation demand (ET) contributes to the decreasing trend in PmE (Fig.4c).

As for the future projection, precipitation shows a recovery since the 2020s in all scenarios except SSP3-7.0 under which it recovers from the 2030s. Changes in precipitation return to the ranges of natural variability around 2030 (2025~2035), 2037 (2031~2043), 2059 (2054~2064), 2039 (2032~2046) in SSP1-2.6, SSP2-4.5, SSP3-7.0, and SSP5-8.5, respectively (colored lines in Fig.4a), and even exceeds internal variability around 2080 in SSP5-8.5. In comparison, ET in all scenarios keeps on increasing with a faster rate under stronger anthropogenic forcing (Fig.4b). The changes in PmE under SSP2-4.5 and SSP3-7.0 do not return to the ranges of internal variability because of faster ET increase and moderated recovery of precipitation with global warming (Table S3). The changes in precipitation, ET and PmE demonstrate that future global warming benefits a recovery of Southeast Asian monsoon precipitation, but faster ET increase could overwhelm its recovery and contribute to a further decrease in PmE and higher drought risk.

Similar to drought changes, the earliest TOE of decreased precipitation is also seen over Southwest China (Fig.S7a-b). Under SSP1-2.6, SSP2-4.5 and SSP5-8.5, eastern part of South China and Mekong River would return to the ranges of natural variability around 2040 (Fig.S7c-f). Under SSP3-7.0, the area with precipitation returning to internal variability is the smallest (Fig.S7e).

Enhancement of precipitation in the future projection is closely related to radiative forcing. In Hist, reduction in precipitation is dominated by anthropogenic aerosol forcing by reducing atmospheric humidity and weakening the monsoon circulation, although the thermodynamic effect from greenhouse gases forcing can partly offset the impact of anthropogenic aerosol forcing (Zhou et al., 2020). In the future projection, greenhouse gases (GHGs) keep on increase but anthropogenic aerosol forcing declines (O'Neill et al., 2016), which intensifies the impact of GHGs on precipitation through the thermodynamic response (Chen et al., 2020; Wilcox et al., 2020), and enhances ET as well. Higher scenarios result in faster warming, and faster recovery in precipitation and enhancement in ET. Only under SSP1-2.6 and SSP5-8.5, the recovery of precipitation exceeds enhanced ET, favorable of less drought risk and a return to the variability in a natural world.

4. Summary and conclusion remarks

As a slow-onset extreme event, drought over Southeast Asian monsoon region is paid less attention so far. We examined drought changes over this region in the observation from 1950 to 2018, and showed that Southeast Asian monsoon region has been undergoing more frequent and more wide-spread drought for 1951-2018 in the observation, centered Southwest China, northern Thailand and Myanmar. The extreme drought affected area fraction are almost doubled during 1951-2018 over the study region.

The impact of anthropogenic forcing and projected changes in drought under different scenarios were investigated by comparing Hist and future projections with piControl from the CMIP6 multimodel output. We found a detectable role of anthropogenic forcing on the increasing drought risk over the Southeast Asian monsoon region. Human influence has increased the occurrence and affected area fraction of extreme drought during 1951-2014. Consistent with the observation, significant increasing trends for the drought occurrence and affected area fraction in Hist are simulated since the early 20^{th} century. The TOE of extreme drought occurrence and affected area appeared around 1967 (1928~2006) and 1967 (1941~1993), respectively. The anthropogenic forced precipitation decrease dominates the increasing drought risk in the past century. In the future, the projected changes in extreme and severe drought risk would start to decrease around the 2030s under SSP1-2.6, while keep on increasing through the whole 21^{st} century under SSP3-7.0 and SSP5-8.5. However, the projected changes in drought risk under all scenarios are still beyond the ranges of natural variability.

Our study demonstrated a distinguishable role of anthropogenic forcing in the increasing drought risk over Southeast Asian monsoon region, and the TOE of anthropogenic forcing on drought has occurred in the past. Both higher aerosols loading and higher radiative forcing in the future are important for the drought changes, and SSP3-7.0, which bears the largest anthropogenic aerosol loadings in the future and second high radiative forcing among the four scenarios, projects the most frequent and most widespread drought for the mid- and long-term projections. Although precipitation over Southeast Asian monsoon region will recover since the 2050s due to more atmospheric humidity with global warming, the evapotranspiration enhancement could offset and even overwhelm the precipitation recovery, increasing the drought risk.

Southeast Asian monsoon region, particular over the Mekong river Basin, will be the hotspot of frequent and widespread drought risk in the future. It would greatly threaten the agriculture, heightened fire risks and lead to acute shortages of drinking water. ASEAN and the United Nations Economic and Social Commission for Asia and the Pacific proposed to build resilience to drought in Southeast Asia mitigate the impacts of drought (UN, 2020). Here, we demonstrate the choice of pathways is also crucial for the drought risk changes over Southeast in the future. It is urgent to take actions to reduce anthropogenic aerosol loading and greenhouses gases emissions to reduce the Southeast Asian drought risks.

Acknowledgement:

This work was jointly supported by the Ministry of Science and Technology of China under Grant 2018YFA0606501 and National Natural Science Foundation of China under grant No. 42075037. We acknowledge the World Climate Research Programme's Working Group on

Coupled Modeling, which is responsible for CMIP6, and the climate modeling groups (listed in Table S1) for producing and making available their model output (https://esgf-node.llnl.gov/search/cmip6/). We also thank University of East Anglia Climatic Research Unit (CRU) for providing the observational precipitation datasets (https://catalogue.ceda.ac.uk/uuid/10d3e3640f004c578403419aac167d82). The SPEI and sc-PDSI datasets can be freely accessed from the websites (https://spei.csic.es/spei_database.html and https://crudata.uea.ac.uk/cru/data/drought/). Surface soil moisture from GLDAS is available from https://disc.gsfc.nasa.gov/datasets/GLDAS_NOAH025_M_2.1/summary.

References:

Amnuaylojaroen Teerachai and Pavinee Chanvichit (2019) Projection of near-future climate change and agricultural drought in Mainland Southeast Asia under RCP8.5. Climatic Change, 155:175-193.

Beaudoing, H. and M. Rodell, NASA/GSFC/HSL (2019), GLDAS Noah Land Surface Model L4 monthly 0.25 x 0.25 degree V2.0, Greenbelt, Maryland, USA, Goddard Earth Sciences Data and Information Services Center (GES DISC), Accessed: [https://disc.gsfc.nasa.gov/datasets/GLDAS_NOAH025_M_2.1/summary, last accessed on 25th January 2021], 10.5067/9SQ1B3ZXP2C5

Chen H, and J Sun (2015) Changes in Drought Characteristics over China Using the Standardized Precipitation Evapotranspiration Index. J. Climate, 28, 5430–5447.

Chen Z. M., T. J. Zhou, L. X. Zhang, et al. (2020) Global land monsoon precipitation changes in CMIP6. Geophysical Research Letters, 47, e2019GL086902. https://doi.org/10.1029/2019GL086902

Cook B. I., J.E. Smerdon, R. Seager., et al. 2014: Global warming and 21st century drying. Clim. Dyn. 43: 2607-2627.

Cook B. I., Mankin, J. S., Marvel, K., Williams, A. P., Smerdon, J. E., & Anchukaitis, K. J. (2020) Twenty-first century drought projections in the CMIP6 forcing scenarios. Earth's Future. 8, e2019EF001461. https://doi.org/10.1029/2019EF001461

Dai A. (2011) Drought under global warming: A review Wiley Interdiscip. Rev. Clim. Chang. 2 45–65.

Droogers P. and R. Allen (2002) Estimating reference evapotranspiration under inaccurate data conditions. Irrigation and Drainage Systems 16: 33–45.

Eyring, V., Bony, S., Meehl, G. A., Senior, C. A., Stevens, B., Stouffer, R. J., and Taylor, K. E. (2016) Overview of the Coupled Model Intercomparison Project Phase 6 (CMIP6) experimental design and organization, Geosci. Model Dev., 9, 1937–1958, https://doi.org/10.5194/gmd-9-1937-2016.

Hariadi M. H. (2017) Projected drought severity changes in Southeast Asia under medium and extreme climate change. Wageningen University and Research, and Royal Netherlands Meteorological Institute, Ministry of Infrastructure and the Environment, KNMI Scientific Report WR-2017-02. (M.Sc. thesis report). Available from:

http://bibliotheek.knmi.nl/knmipubWR/WR2017-02.pdf.

Harris I., T. J. Osborn, P. Jones, and D. Lister (2020) Version 4 of the CRU TS monthly high-resolution gridded multivariate climate dataset. Scientific Data, 7, 109(2020). https://doi.org/10.1038/s41597-020-0453-3

Juneng, L. and Tangang, F. (2005) Evolution of ENSO-related rainfall anomalies in Southeast Asia region and its relationship with atmosphere–ocean variations in Indo-Pacific sector, Clim. Dyn., 25, 337–350.

Kumar M. D., P. K. Viswaathan and Nitin Bassi (2015) Water Scarcity and Pollution in South and Southeast Asia: Problems and Challenges, in Paul G. Harris and Graeme Lang (eds.), Routledge Handbook of Environment and Society in Asia, Routledge, Taylor & Francis Group, London, pp. 197-215.

O'Neill, B. C., Tebaldi, C., van Vuuren, D.P., Eyring, V., Friedlingstein, P., Hurtt, G., Knutti, R., Kriegler, E., Lamarque, J.-F., Lowe, J., Meehl, G.A., Moss, R., Riahi, K., and Sanderson, B. M. (2016) The Scenario Model Intercomparison Project (ScenarioMIP) for CMIP6. Geosci. Model Dev., 9: 3461-3482.

Räsänen, T. A. and Kummu, M.(2013) Spatiotemporal influences of ENSO on precipitation and flood pulse in the Mekong River Basin, J. Hydrol., 476, 154–168.

Rodell, M., P.R. Houser, U. Jambor, J. Gottschalck, K. Mitchell, C. Meng, K. Arsenault, B. Cosgrove, J. Radakovich, M. Bosilovich, J.K. Entin, J.P. Walker, D. Lohmann, and D. Toll, 2004: The Global Land Data Assimilation System, Bull. Amer. Meteor. Soc., 85, 381-394, doi:10.1175/BAMS-85-3-381

Schrier G. van der, J. Barichivich, K. R. Briffa, P. D. Jones (2013) A scPDSI-based global data set of dry and wet spells for 1901-2009. J. Geophys. Res. Atmos., 118, 4025–4048, doi:10.1002/jgrd.50355.

Sodhi, N. S. et al. (2010) The state and conservation of Southeast Asian biodiversity. Biodivers. Conserv. 19, 317–328.

Stibig, H. J., Achard, F., Carboni, S., Rasi, R. & Miettinen, J. (2014) Change in tropical forest cover of Southeast Asia from 1990 to 2010. Biogeosciences 11, 247–258.

Trenberth, K. E., A. Dai, G. van der Schrier, P. D. Jones, J. Barichivich, K. R. Briffa, and J. Sheffield (2014) Global warming and changes in drought. Nature Climate Change, 4, 17-22

Ukkola A. M., M. G. D. Kauwe, M. L. Roderick, G. Abramowitz, A. J. Pitman (2020) Robust Future Changes in Meteorological Drought in CMIP6 Projections Despite Uncertainty in Precipitation. Geophysical Research Letters, 47, e2020GL087820, https://doi.org/10.1029/2020GL087820.

Vicente-Serrano S.M., Beguería S., López-Moreno J.I., (2010a) A Multi-scalar drought index sensitive to global warming: The Standardized Precipitation Evapotranspiration Index-SPEI. Journal of Climate, 23(7), 1696-1718, DOI: 10.1175/2009JCLI2909.1. http://digital.csic.es/handle/10261/22405.

Vicente-Serrano S.M., Beguería S., López-Moreno J.I., Angulo M., El Kenawy A. (2010b) A global 0.5° gridded dataset (1901-2006) of a multiscalar drought index considering the joint effects of precipitation and temperature. Journal of Hydrometeorology 11(4), 1033-1043, DOI: 10.1175/2010JHM1224.1. http://digital.csic.es/handle/10261/23906.

Wang B., M. Biasutti, M. P. Byrne, et al. (2020) Monsoon Climate Change Assessment. Bull. Amer. Meteor. Soc., https://doi.org/10.1175/BAMS-D-19-0335.1.

Wang Lin, Chen Wen, Zhou Wen, Huang Gang (2015) Understanding and detecting super extreme droughts in Southwest China through an integrated approach and index. Q. J. R. Meteorol. Soc., 142: 529–535, DOI: 10.1002/qj.2593.

Wells N., Goddard S. and Hayes M.J. (2004) A self-calibrating Palmer Drought Severity Index. Journal of Climate, 17, 2335-2351

Xin X., R. Yu, T. Zhou, and B. Wang (2006) Drought in late spring of South China in recent decades. J. Climate, 19, 3197–3206, https://doi.org/10.1175/JCLI3794.1.

Zhang H., & Delworth, T. L. (2018). Robustness of anthropogenically forced decadal precipitation changes projected for the 21st century. *Nat Commun, 9*(1), 1150. https://doi.org/10.1038/

Zhang L., Zhou T., Chen X., Wu P., Christidis N., Lott F. (2020). The late spring drought of 2018 in South China, Bull. Amer. Met. Soc., 101(1): S59-S64. DOI:10.1175/BAMS-D-19-0202.1.

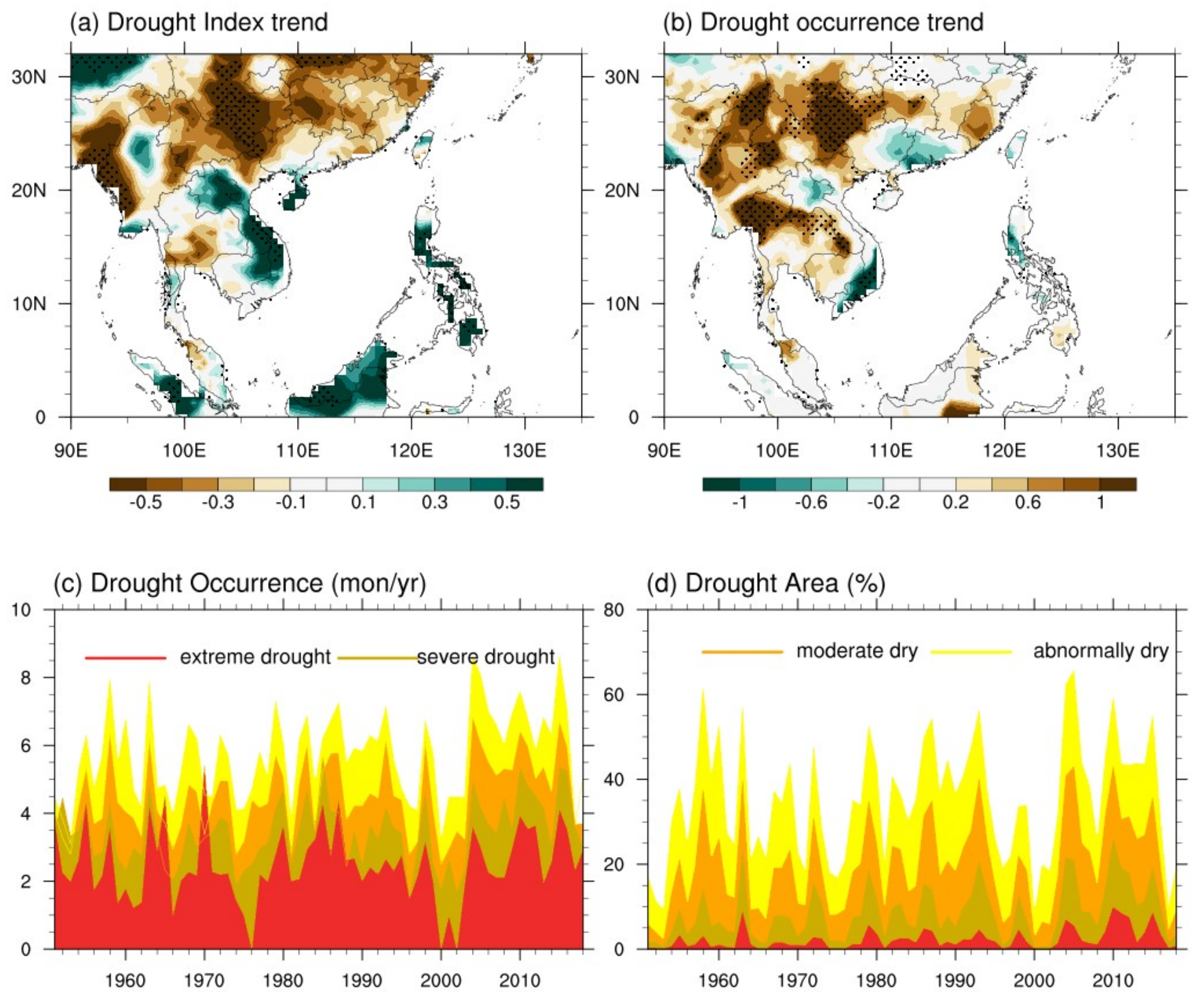

Fig. 1 The spatial distribution for observed linear trend of drought from 1951 to 2018 for (a) SPEI (unit: $(68yr)^{-1}$) (b) extreme drought (SPEI≤-2.0) occurrence (unit: month $(68yr)^{-1}$). (c)-(d) are the temporal changes of (c) occurrence (unit: month yr^{-1}) and (d) affected area fraction (unit: %) for different drought categories averaged over Southeast Asian monsoon region (10-30°N, 90-120°E). The yellow, orange, brown and red lines represent abnormally dry (SPEI≤-0.5), moderate drought (SPEI≤-1.0), severe drought (SPEI≤-1.5), and extreme drought (SPEI≤-2.0), respectively.

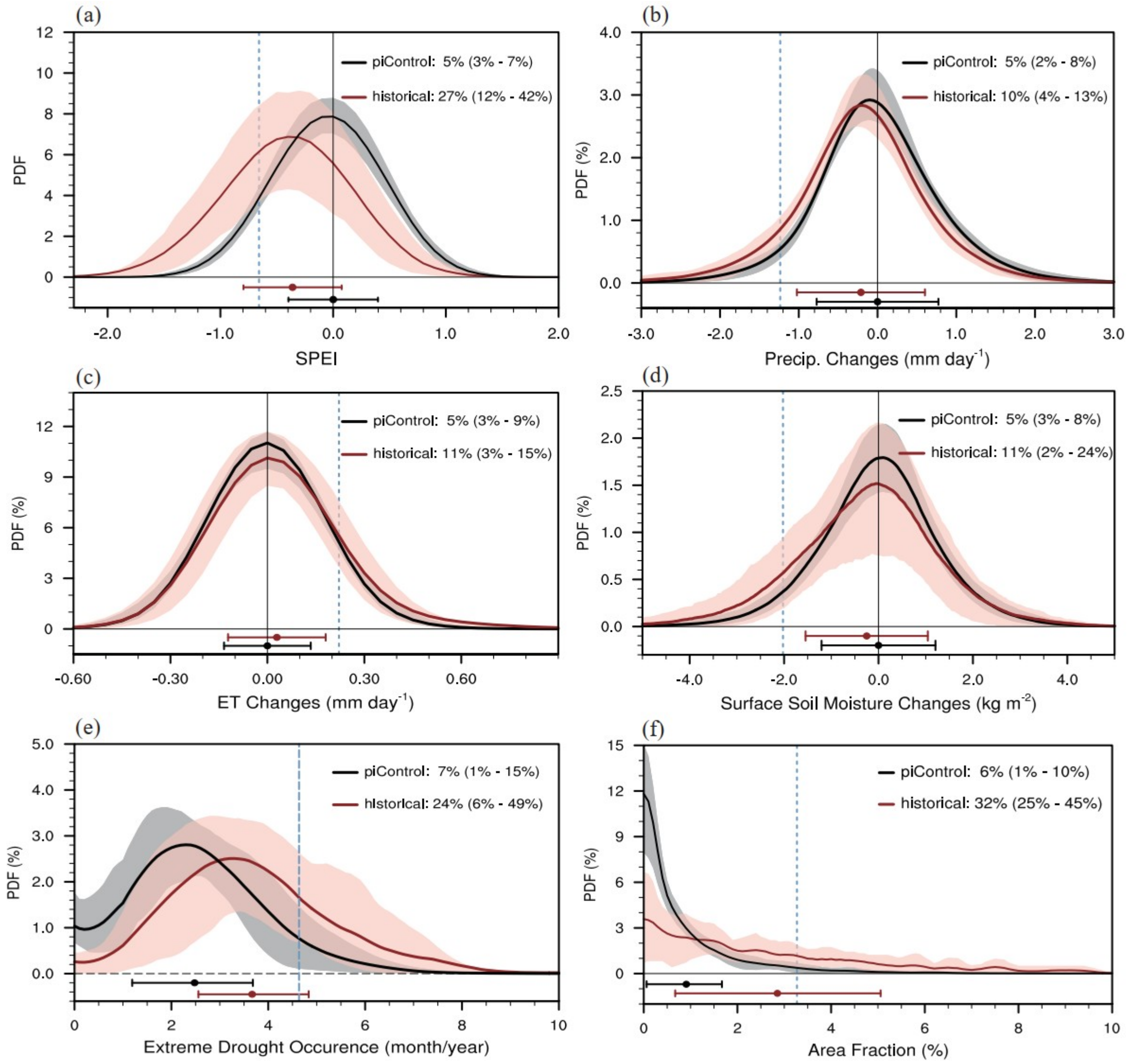

Fig.2 Probability distribution function (PDF) of drought changes in piControl and Hist. (a) SPEI averaged over the land area of Southeast Asian monsoon region. (b)-(c) are same as (a), but for annual mean precipitation (mm day^{-1}), ET (mm day^{-1}) and surface soil moisture (0-10cm) (kg m^{-2}) anomalies relative to piControl. (e)-(f) are for extreme drought occurrence and affected area fraction over the Southeast Asian land monsoon region. The solid lines are the multi-model ensemble (MME) mean of piControl (black line) and Hist for 1950-2014 (red line), and the shadings denote the range of 10th to 90th across models. The vertical blue dash lines denote the return value of 20-yr period. The horizontal lines and dots denote the range of standard deviation and the mean value of PDFs, respectively. The mean value and the inter-model 10th-90th range are shown in the right corner of each plot.

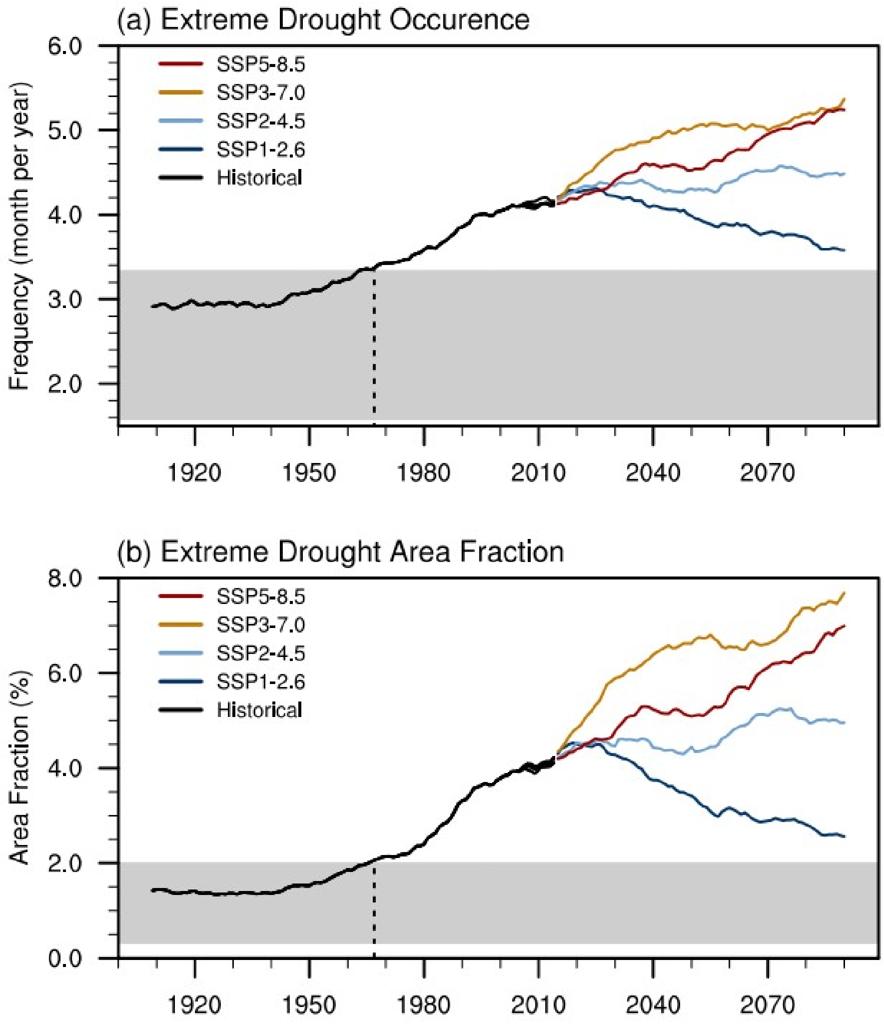

Fig.3 The 20-yr running mean changes in extreme drought (a) occurrence (month year^{-1}) and (b) affected area fraction (%) over the Southeast Asian monsoon region in Hist (black) and four future projections (colored lines) based on multi-model ensemble (MME) of the 14 CMIP6 models. The gray shadings denote the range of internal variability, which has been corrected by the ratio between the standard deviation of observation and Hist in 1950~2014 (FigS5). The dark blue, light blue, brown and red are for SSP1-2.6, SSP2-4.5, SSP3-7.0 and SSP5-8.5, respectively. The black vertical dash lines denote the time of emergence (TOE).

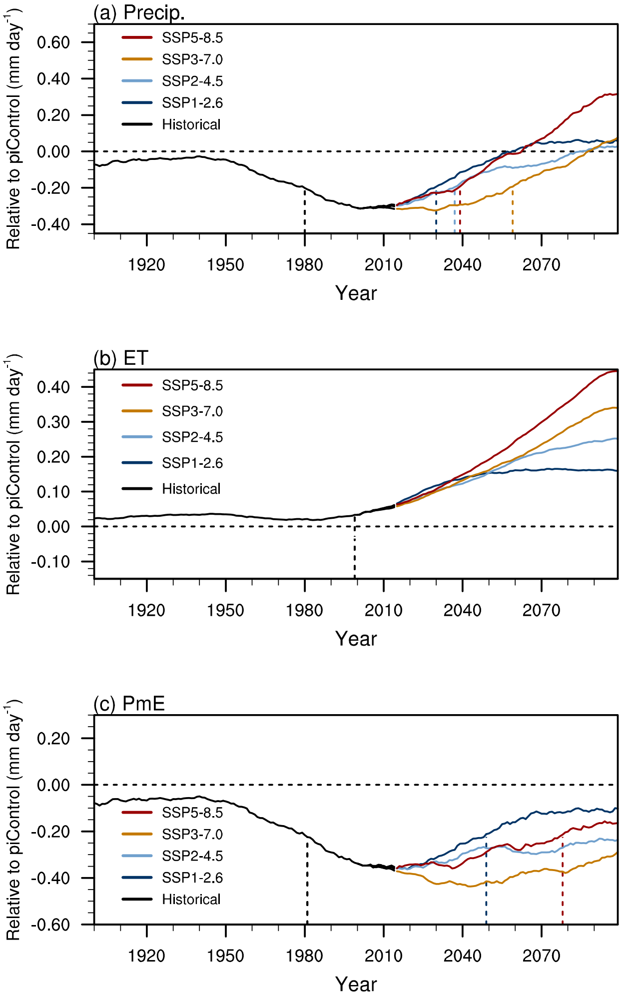

Fig. 4 Same as Fig.3, but for the changes in anomalous annual mean (a) precipitation (P), (b) evapotranspiration (ET) and (c) P minus ET (PmE) area-averaged over the Southeast Asian monsoon region relative to piControl.